Journal of Natural Gas Science and Engineering 60 (2018) 1–10

Contents lists available at ScienceDirect

Journal of Natural Gas Science and Engineering

journal homepage: www.elsevier.com/locate/jngse

Delineation of early Jurassic aged sand dunes and paleo-wind direction in southwestern Wyoming using seismic attributes, inversion, and petrophysical modeling

Sumit Verma[a,*], Shuvajit Bhattacharya[b], Brady Lujan[a], Dhruv Agrawal[a], Subhashis Mallick[c]

[a] Geology Program, The University of Texas of the Permian Basin, Odessa, TX, USA
[b] Department of Geological Sciences, University of Alaska, Anchorage, AK, USA
[c] Department of Geology and Geophysics, School of Energy Resources, University of Wyoming, Laramie, WY, USA

ARTICLE INFO

Keywords:
3D Seismic
Paleowind direction
Nugget Sandstone
Seismic attributes

ABSTRACT

Moxa Arch is a potential site for carbon sequestration in the state of Wyoming, recognized by the US Department of Energy. In this paper, we primarily focus on improving our understanding of the geology, including lithofacies and depositional environment, of Nugget Sandstone-a potential carbon storage reservoir, by integrating results from three different techniques including seismic attributes, seismic inversion, and petrophysical modeling. The Nugget Sandstone formation is primarily an eolian sandstone, deposited in the early Jurassic and is present throughout southwestern Wyoming. Seismic attribute analysis indicates the presence of NW-SE trending elongated geological features in the Nugget Sandstone interval. Based on our seismic and well log analyses, we interpret these features to be eolian sand dunes, which is consistent with the previous publications indicating a general NE-SW paleo-wind direction at the time of the deposition of Nugget Sandstone and other equivalent formations in Wyoming and Utah. The petrophysical analysis indicates that the Nugget Formation is mostly composed of quartz; however, clay and evaporites such as anhydrite and halite are also present. The acoustic impedance, derived from well logs, indicates that high porosity dunal sandstones correspond to low impedance values whereas interdunal evaporites are characterized by high impedance values. Combined analysis of seismic attribute coherence and inverted P-impedance discriminates the dunal and interdunal deposits in 3D seismic data volume; the low coherence defines the extent of low impedance dunal deposits. Detailed analysis of the curvature attribute from the seismic data indicates a dominant paleo-wind direction of approximately N225°.

1. Introduction

Our study area is located in southwestern Wyoming on top of the Moxa Arch, which is a gently dipping and doubly plunging anticline (~5°), extending from the south of the Uinta Mountains at the Utah/Wyoming border and go north up to the town of La Barge, Wyoming (Fig. 1). Moxa Arch and Rock Springs Uplift (RSU) were identified as two potential sites for carbon sequestration by the US Department of Energy (DOE). There has been significant research done on the RSU as a carbon sequestration site, whereas the Moxa Arch is less studied (Grana et al., 2017; Sharma et al., 2018; Surdam, 2013; Mallick and Adhikari, 2015; and Verma et al., 2016 among others). The Moxa Arch has several potential storage reservoirs including the Jurassic Nugget Sandstone, the Mississippian Madison Limestone, and the Ordovician Bighorn Dolomite. In the study area, an oil and gas company has been injecting CO_2 and H_2S in the Madison Limestone on the Moxa Arch, at the Shute Creek processing facility for over 10 years. The Nugget Sandstone is a heterogeneous and anisotropic eolian deposit, and is a producing formation in some parts of the Moxa Arch, which can be a challenge for its consideration as its potential for carbon storage. At the same time, Nugget Sandstone is a relatively shallow formation as compared with other potential storage formations (such as the Madison Limestone formation) in the area. Therefore, if proven as good storage reservoir, it would be a cheaper alternative for carbon storage than the other formations. Our survey location is critical, since the Naughton Power Plant, a coal-fired power station which emits up to 6 Mt of CO_2 per year, lies approximately 20 miles south-west of our study area (Campbell-Stone et al., 2011). This paper is focused on developing the geological understanding of the Nugget Sandstone and its potential for carbon storage.

Nugget sandstone in southwestern Wyoming is a lower Jurassic eolian sand deposit, and is equivalent to the Navajo Sandstone of

* Corresponding author.
E-mail address: verma_s@utpb.edu (S. Verma).

https://doi.org/10.1016/j.jngse.2018.09.022
Received 27 March 2018; Received in revised form 16 August 2018; Accepted 25 September 2018
Available online 28 September 2018
1875-5100/ Published by Elsevier B.V.

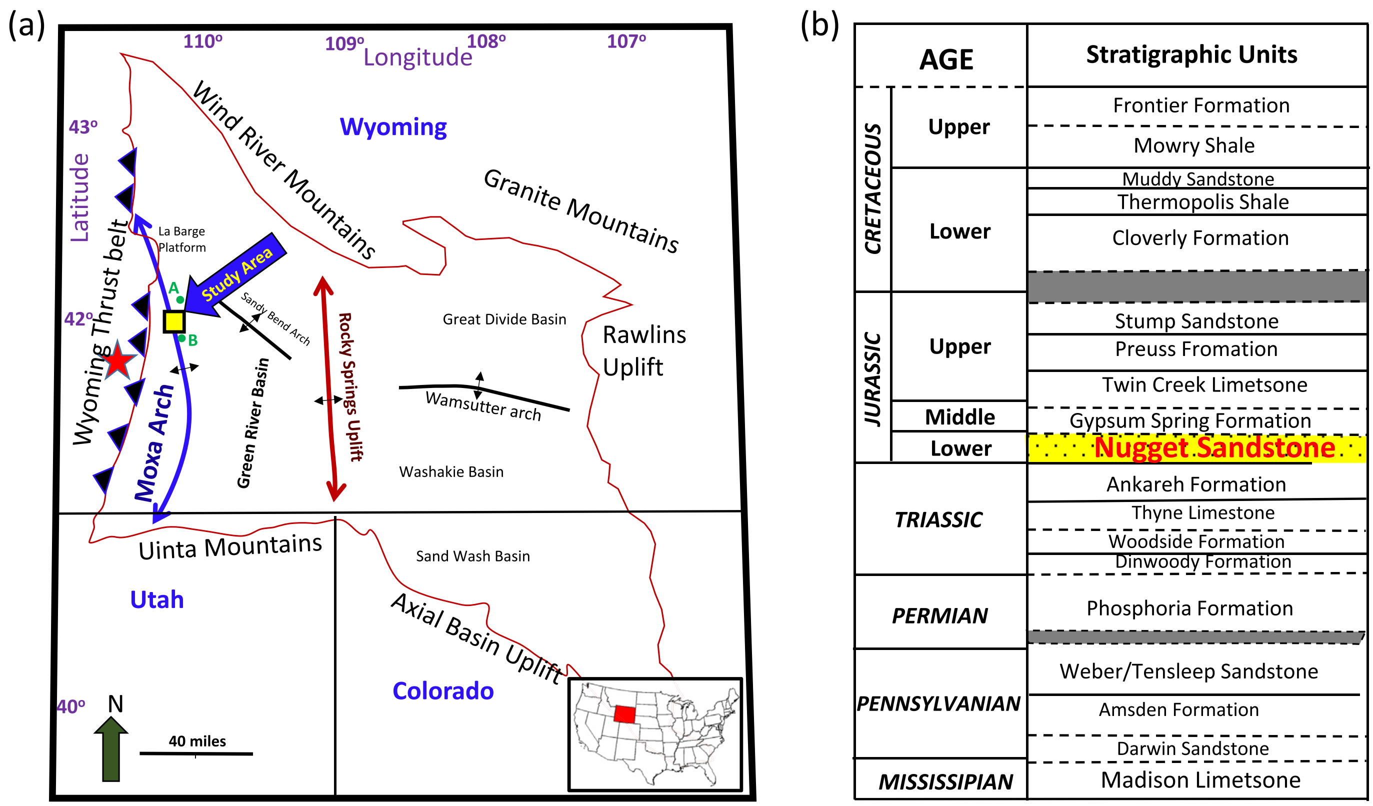

Fig. 1. (a) Location map of the Moxa Arch and Rock Springs Uplift in SW Wyoming (modified after Verma et al., 2016). The green dots next to the survey represent the approximate well location. A = Keller 1-12, and B = AGI 2-18 are the wells used for the study. The red colored star represent the location of the Naughton Power Plant. (b) Generalized stratigraphy of the Moxa Arch (modified after Thyne et al., 2010). (For interpretation of the references to color in this figure legend, the reader is referred to the Web version of this article.)

southwestern Utah. Loope and Rowe (2003) compared Arizona, Utah, and Wyoming during the early Jurassic period with the present day Sahara Desert. Nugget Sandstone was deposited in a subtropical dune field in the present day northern Utah and southern Wyoming (Fig. 2a). Navajo sandstone, which is outcrops in several locations in Utah, has been heavily studied (Parrish and Peterson, 1988; Chan and Archer, 2000). Parrish and Peterson (1988) identified the wind direction for Nugget, Navajo and Aztec Sandstones (Fig. 2b) by analyzing their outcrops.

Seismic attributes can help us understand varying subsurface geological and stratigraphic features. Out of various attributes available in seismic literature, coherence and curvature attributes has been used in past to delineate different stratigraphic and structural features such as different types of channels, faults, folds and karst (Chopra and Marfurt, 2007; Qi et al., 2014, 2017; Khoudaiberdiev et al., 2017) However, paleo sand dunes were not particularly studied using these attributes. In our study, we analyze the seismic attributes, primarily curvature and coherence, to identify the shape of the paleo-sand dunes and attempt to identify wind direction during the time of the paleo-wind deposition. We also analyze well logs to understand the petrophysical properties of dunal and interdunal deposits. Further, we perform a post-stack seismic inversion, followed by an integrated analysis of seismic attributes, well logs, and seismic inversion results to identify dunal and interdunal deposits.

2. Geology of the study area

2.1. Moxa Arch

The Moxa Arch is an anticline stretching from the southern portion of the La Barge Platform to just north of the Uinta Mountains. In the northern part of the arch, and within our study area, the axis of the arch trends northwest to southeast but then changes to a northeast to southwest trend in the southern portion of the arch close to the Uinta Mountains. Because of its size and structural closure, the Moxa Arch has been the target of extensive hydrocarbon exploration since the 1960s with major gas and oil reservoirs being discovered all along the arch. Structurally, the Moxa Arch is a basement involved anticlinal structure with gently dipping arms that were created as the Wyoming thrust belt developed during the Laramide orogeny (Verma et al., 2016; Campbell-Stone et al., 2011). Moxa Arch contains approximately 22,000 ft (6.7 km) sedimentary strata above Precambrian basement. Mississippian Madison Limestone and Jurassic Nugget Sandstone are potential formations for carbon storage (Surdam, 2013). In our study area, the Nugget Sandstone lies at approximately 12,500 ft (3.8 km), and the Madison Limestone at 16,500 ft (5 km) below the surface. For the rest of the paper, we will focus on Nugget Sandstone formation.

2.2. Nugget Sandstone

The Nugget Sandstone is an eolian sandstone, deposited in the early Jurassic and is present across southwestern Wyoming both in the subsurface and as outcrop (Figs. 1b and 2). During the early Jurassic period, the western United States including Arizona, Utah and Wyoming, lied around 15°-25° latitude with the paleo-environment comparable to the present day Sahara Desert (Loope and Rowe, 2003). Based on the consistency of the prevailing wind direction, prevailing wind speed, and sand supply, different types of sand dunes can form. Fig. 2b shows the extent of early Jurassic Nugget Sandstone and Navajo Sandstone deposition. Predominantly eolian processes build these formations; they feature cross-bedded, low-angle to horizontally bedded and rippled, very-fine to coarse-grained sand in dunes, interdune areas, and associated environments (Lindquist, 1983).

Sand dune cross beddings can help in the identification of paleo-

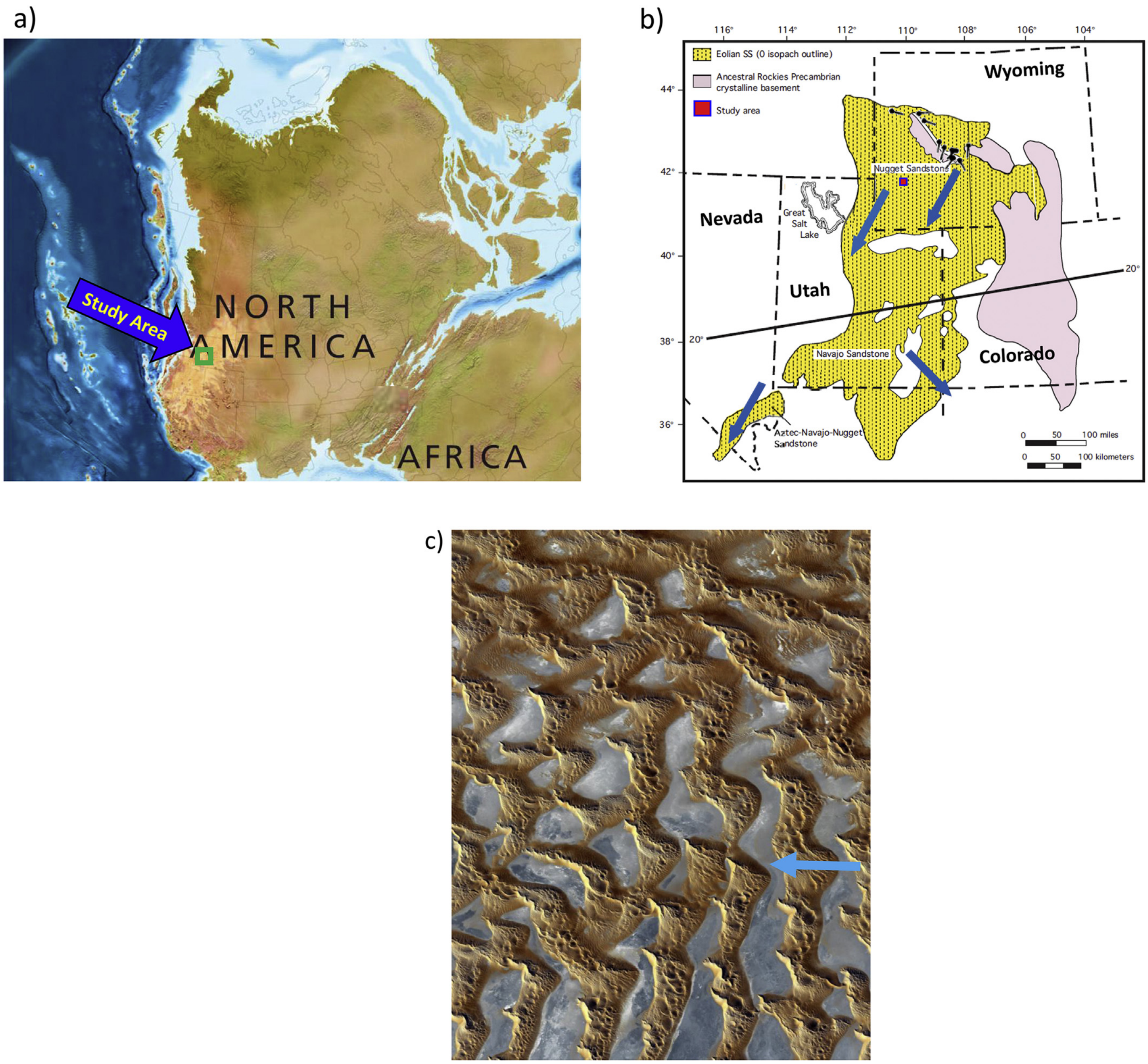

Fig. 2. (a) North American continent during early Jurassic. The green rectangle represents the approximate location of the study area (after National Park Services, 2016). (b) Paleo-wind direction of Nugget and Navajo Sandstone. Note the black dipoles in Wyoming state close to Precambrian uplift showing the outcrop locations of Nugget Sandstone where the wind direction measurement was taken (after Parrish and Peterson, 1988 and Chan and Archer, 2000). (c) Satellite image of Rub' al Khali, Arabia, which is one of the largest desert in the world. The blue arrow shows the general wind direction. The earth yellow color represent the dunal deposits, whereas the blue and white color represent the interdunal area (after ASTER, 2005). (For interpretation of the references to color in this figure legend, the reader is referred to the Web version of this article.)

wind direction. Cross bedding structures are best preserved in “eolian forests” along the leading edges of the dunes. Several authors, including Parrish and Peterson (1988) and Chan and Archer (2000), Loope and Rowe (2003) among others, studied the outcrops of Nugget Sandstone and Navajo Sandstone formations in Arizona, Utah and Wyoming. The cross-bedding orientations indicate that the general wind direction in North America at the time of deposition of Nugget Sandstone was NE-SW. Chan and Archer (2000) measured a continuous series of 297 concordant cyclic cross-beds which indicated a south-southwesterly paleoflow of N200° to N201°. Fig. 2b shows the wind direction, to be NE-SW with some exceptions. One of the exceptions is the outcrop close to the northern edge of Nugget Sandstone in the central Wyoming. Black tadpoles on Fig. 2b show the wind direction at the outcrop study location. These tadpoles indicate that, the paleo-wind direction varies from west to east to northeast to southwest. Parrish and Peterson (1988) suggest that, at the locations which show westward wind direction (the three northern-most measurements on Fig. 2b), the measurements were made on bottom-most bed of the Nugget Sandstone.

3. Data analysis

3.1. Seismic and well log data

For our study, we had access to a 3D seismic survey and three well logs. The 3D seismic survey was acquired in 1999 with dynamite source, 5 s record length, with a maximum offset range of 14,500 ft and

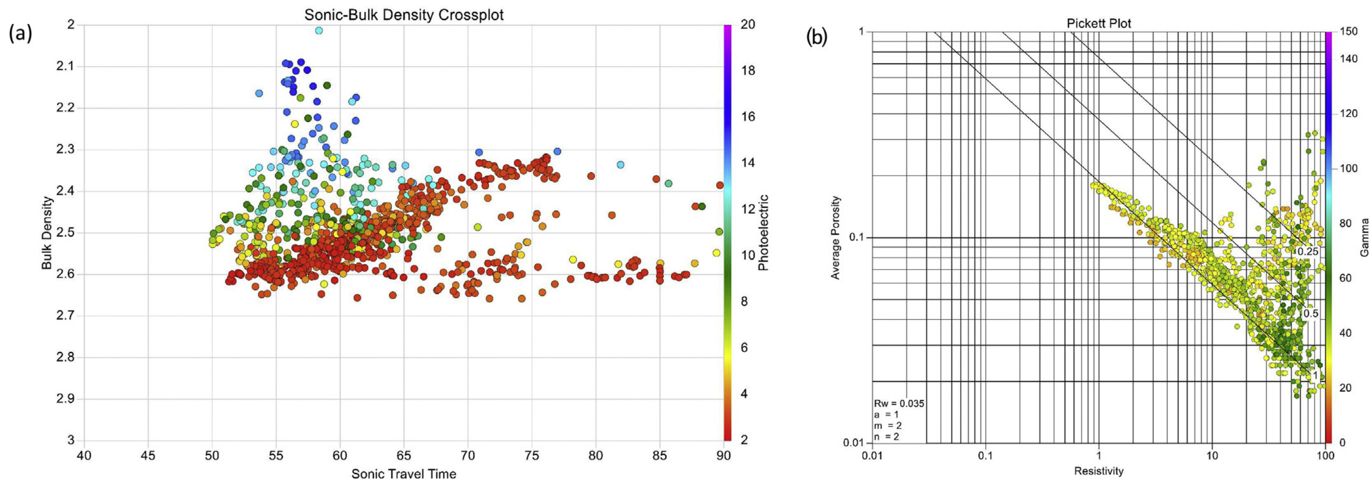

Fig. 3. (a) Sonic-bulk density crossplot color-coded by photo-electric curve shows heterogeneities present in the Nugget Sandstone formation. (b) Pickett plot color-coded by gamma-ray curve showing lines at different water saturation values, such as 100%, 50%, and 25% in the Nugget Sandstone formation. The parameters used in the Archie equation for water saturation calculation are shown in the figure. AGI 2-18 well logs were used for the crossplots. (For interpretation of the references to color in this figure legend, the reader is referred to the Web version of this article.)

covering approximately 36 mi^2 in area (Figs. 1a and 4a). There are no wells in the area which were deep enough to penetrate the zone of interest. We used two available wells (Keller 1–12 and AGI 2–18) that are located nearest to the area of the seismic survey. Keller 1–12 well lies approximately 3 miles from the seismic survey in the northeast direction, while AGI 2–18 is situated around 4.5 miles away in the southeast direction.

3.2. Petrophysical analysis

We used common triple-combo logs from the available wells to perform basic and advanced petrophysical analyses of the Nugget Sandstone formation. We identified general lithology, fluid content, and estimated fluid saturation using common well log patterns and cross-plots. We identified the Nugget Sandstone as an overall sandstone formation based on its low gamma signature and higher density porosity values than neutron porosity. However, the formation shows occasional peaks in the gamma-ray curve, which can be attributed to the presence of clay. Next, we used different cross-plots, such as sonic-bulk density and Pickett plot to better understand the lithology and compute fluid saturation (Fig. 3a and b). Sonic-bulk density crossplot color-coded by photo-electric log (Fig. 3a) revealed the presence of minerals with very low density (< 2.2 g/cc), high photo-electric values, and relatively higher velocity than the majority of the samples. This pattern is indicative of a few minerals in the evaporites group (e.g. halite and sylvite) commonly present in sand dunes. In the next step, we generated a Pickett plot (Fig. 3b) to identify the fluid type and derive required parameters for Archie-based water saturation estimation (Archie, 1942). Pickett plot is a graphical technique that uses resistivity and average porosity (computed from neutron and density porosity) values. On the Pickett plot the 100% water saturation line can be observed. The value of average porosity, at the point where 100% water saturation line crosses the porosity axis, can be quantified as water resistivity (Rw) multiplied by tortuosity (a). The plot showed that most of the samples from the Nugget Sandstone formation are water-bearing. The slope of the constructed lines at different water saturation (100%, 50%, and 25%) can be used to determine the values of cementation factor (m) as needed in the Archie equation (Rider and Kennedy, 2011). The values of a, m, n, and Rw in the Archie equation were 2, 2, 1, and 0.035 ohm-m, respectively.

We performed petrophysical inversion and obtained statistical multi-mineralogical solutions for AGI 2–18 and Keller 1–12 wells, using common well logs (Savre, 1963; Moss and Harrison, 1985; Mitchell and Nelson, 1988; Kulyapin and Sokolova, 2014). Such inversion helps us better understand the mineralogical composition and facies variability in the Nugget Sandstone formation at well-log scale. We used the available mudlogs in the wells to augment the quality of petrophysical inversion-based multi-mineralogical solution. Input well logs selected for the statistical multi-mineralogical solutions were: gamma, neutron-porosity, bulk density, and Umaa (Umaa is the product of photoelectric and density log corrected by apparent total porosity). Calculated output curves are the volumetric proportions of quartz, illite, kaolinite, calcite, dolomite, anhydrite, halite, gypsum, and bulk volume water (Fig. 4a). We used standard values of gamma, neutron porosity, bulk density, and Umaa logs for each mineral to generate corresponding synthetic logs. Further, we compared synthetic logs at different mineralogical proportions to the actual well log response from the Nugget interval. We optimized the mineral type, parameters, and the number of iterations to obtain the precise multi-mineral solution with minimum error ($< 2\%$). The computed error is the difference of synthetic log and actual well log.

The statistical mineral solution reveals that the Nugget Sandstone formation is complex, and it is composed of multiple minerals that cannot be visualized easily with basic well log analysis techniques. Although the formation is mostly composed of quartz (> 50–60%), it contains clay, carbonate, halite, anhydrite, and gypsum in variable proportions. An anhydrite bed is present near the top of the Nugget Sandstone formation in both wells (i.e. AGI 2–18 and Keller 1–12). A thick halite-anhydrite bed is present in the middle of the Nugget Sandstone formation in the AGI 2–18 well. Halite is more abundant than anhydrite and gypsum. For the Keller 1–12 well, we found mineralogy similar to the AGI 2–18 well; however, the relative proportions of the minerals are different. The Keller 1–12 well shows more abundance of clay relative to the AGI 2–18 well. There are around four zones with high clay content and minimum thickness of 10 feet present in the Keller 1–12 well. These clay-bearing zones may work as potential baffles while planning for fluid storage and utilization such as carbon sequestration.

3.3. Seismic attribute analysis

Using the 3D seismic data, we computed coherence and structural curvature. Coherence attributes can help in delineating boundaries or edges of a geological feature, where seismic will see changes in shape of seismic waveform. We use energy-ratio similarity (a type a coherence), which is the ratio of the energy of the Karhunen-Loéve filtered data

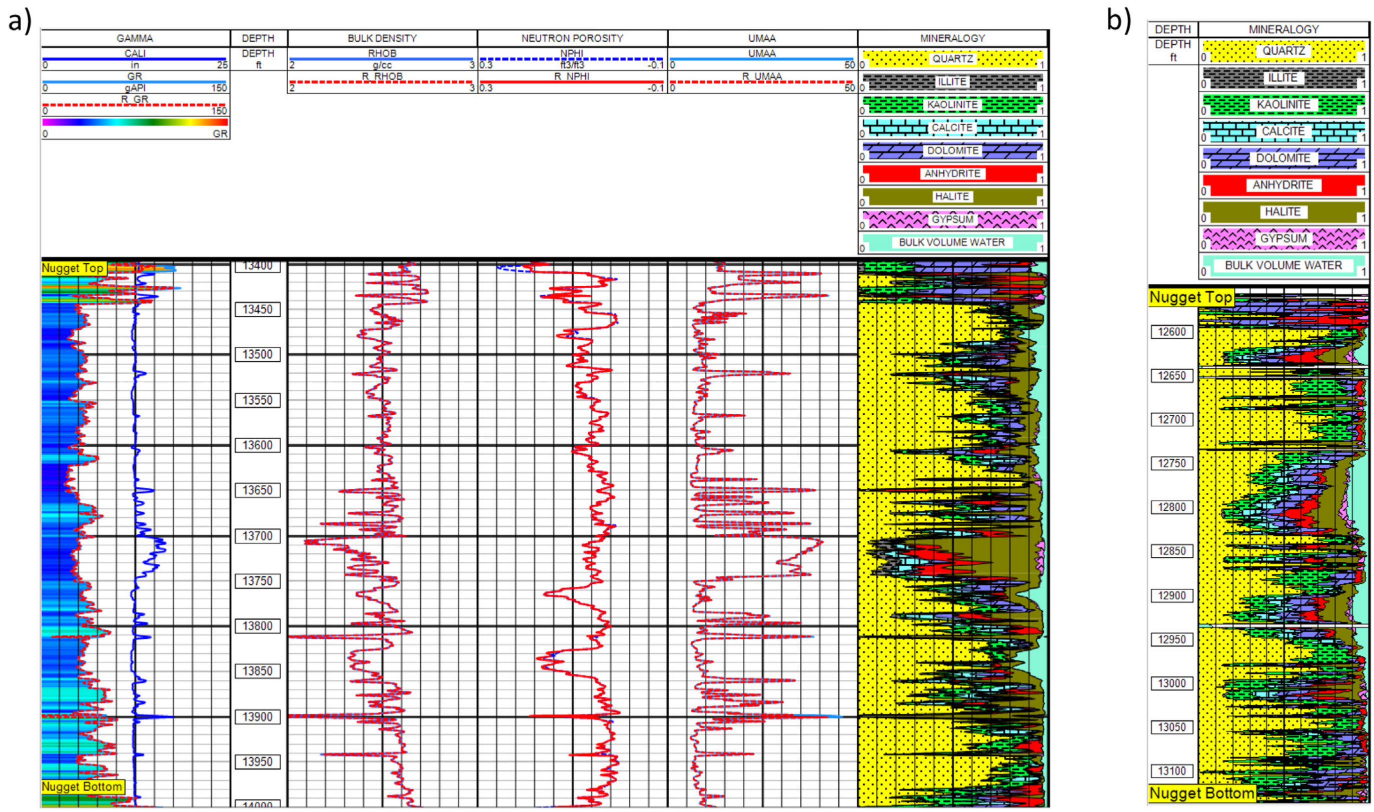

Fig. 4. (a) A statistical mineral solution for the AGI 2-18 well showing actual and synthetic well logs (marked by R). The first four tracks show the common well logs, caliper (CALI), gamma (GR), bulk density (RHOB), neutron porosity (NPHI), and Umaa, and the fifth track shows the multi-mineralogical solution. The overlapping pattern of all synthetic logs on the actual well logs indicates significantly less error in inversion. The Nugget Formation is composed of multiple minerals in different proportions, including quartz, illite, kaolinite, calcite, dolomite, anhydrite, halite, gypsum, and water. (b) Statistical multi-mineral solutions for the well Keller 1–12. Although the solutions indicate the Nugget Formation is predominantly sandstone, there is a significant amount internal heterogeneity present. Based on our analysis, it appears that the AGI 2–18 well is more representative of a sand dunal environment, whereas the Keller 1–12 well suggests more of an interdunal environment.

over the energy of the original unfiltered data (Chopra and Marfurt, 2010). The structural curvature attribute in 2D can be defined as the inverse of the radius of a circle drawn tangent to a curved line (Fig. 5b). The volumetric structural curvature attribute measures the curvedness of the bending and folding of seismic reflector surface. Fig. 5c illustrates that the peak of the antiform is marked as a most positive principal curvature (k_1) anomaly, whereas the most negative principal curvature (k_2) shows anomaly around the trough of the synform (Chopra and Marfurt, 2007).

We analyzed stratal slices of all the computed attributes at three levels- 66 ms (deep), 42 ms (middle) and 26 ms (shallow), below the Nugget Sandstone reflector (Figs. 6 and 7). Coherence and curvature seismic attributes at deep stratal slice (Figs. 6a and 7a) show that the possible sand dune started building up at this level. The middle stratal slice of coherence and curvature (Figs. 6b and 7b) indicates well-developed sand dunes with the major trend of NW-SE. The coherence anomalies mark the boundary between the dunal and interdunal deposits, whereas the positive curvature attribute can help to find the peaks of the sand dunes and negative curvature anomaly can indicate the interdunal areas. The shallow stratal slice of the two attributes indicate that the sand dunes are fading out at this level. We further analyze strike and magnitude of k_1 and generate a 2D hue and saturation plot with strike of k_1 as hue (different colors) and magnitude of k_1 as saturation (different shades of gray, Fig. 8a). The general trend of lineation is NW-SE direction.

3.4. Seismic inversion

We performed a post-stack seismic inversion, which helped in lithology identification. We used the Keller 1–12, which is the nearest well to the survey area, to perform a well to seismic tie. The well to seismic tie correlation was approximately 65% on well A in the zone of interest. The well to seismic tie provided a confirmation that the geologic features seen in Figs. 6 and 7 correspond to Nugget Sandstone formation. Further, in order to perform a post stack seismic inversion, first we created a low frequency model (high pass = 12 Hz and high cut = 15 Hz), with the Keller 1–12 well logs, as well as 3 seismic horizons, including Geophysical Horizon, Nugget Sandstone and Weber Sandstone top (Fig. 5a), marked on 3D seismic volume. Second, we invert the 3D seismic survey for P-impedance using the low frequency model. Fig. 8b shows the P-impedance extracted on the middle stratal slice corendered with coherence. Based on the petrophysical analysis, the low P-impedance corresponds to the porous eolian sand-rich rocks, whereas the high impedance corresponds to the interdunal evaporites. The low coherence anomaly in the figure demarcates the extent of low impedance sand rich facies. The high porosity dunal sandstone facies are indicated by low impedance values with hot colors, whereas the interdunal deposits indicate high impedance with cold colors.

3.5. Seismic facies

We attempted to discriminate between the dunal and interdunal facies using an unsupervised classification method. Here, we used self-organizing maps (SOM) classification technique, which is one of the most used methods of classification in geoscience (Zhao et al., 2016; Roy et al., 2013; Matos et al., 2007; Saraswat and Sen, 2012). We have used, clustered Gray Level Co-occurrence Matrix (GLCM) texture attributes including entropy, energy and homogeneity (Fig. 8c) along

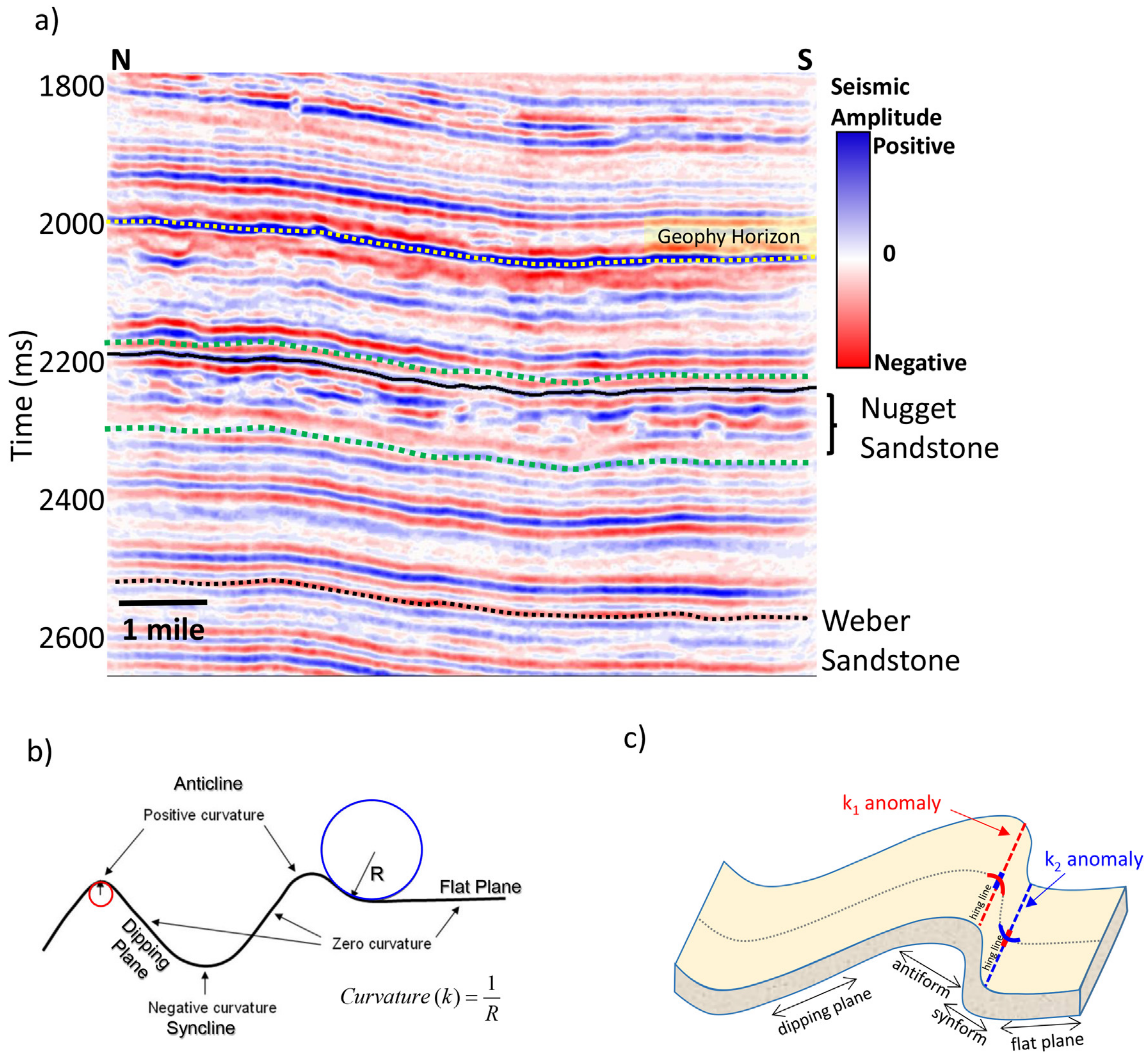

Fig. 5. (a) Seismic amplitude vertical (north-south) section. The Nugget Sandstone formation is approximately 75 ms. The geophysical horizon, on top is a very distinct seismic reflector below Mowry Shale. The Weber Sandstone top is marked as dotted line below Nugget Sandstone. The dotted green lines shows the time window in which Ant Tracking workflow is applied later in this paper. (b) Illustration showing 2D curvature of a curved line. Anticlinal features show positive curvature anomaly, whereas synclinal features show a negative curvature anomaly and planar features (horizontal or dipping) show no curvature anomaly. (c). The illustration shows structural curvature anomaly at an antiform and a synform. The most positive (k_1) and most negative principal curvatures (k_2) anomalies will track the hinge lines which are areas of maximum strain. (For interpretation of the references to color in this figure legend, the reader is referred to the Web version of this article.)

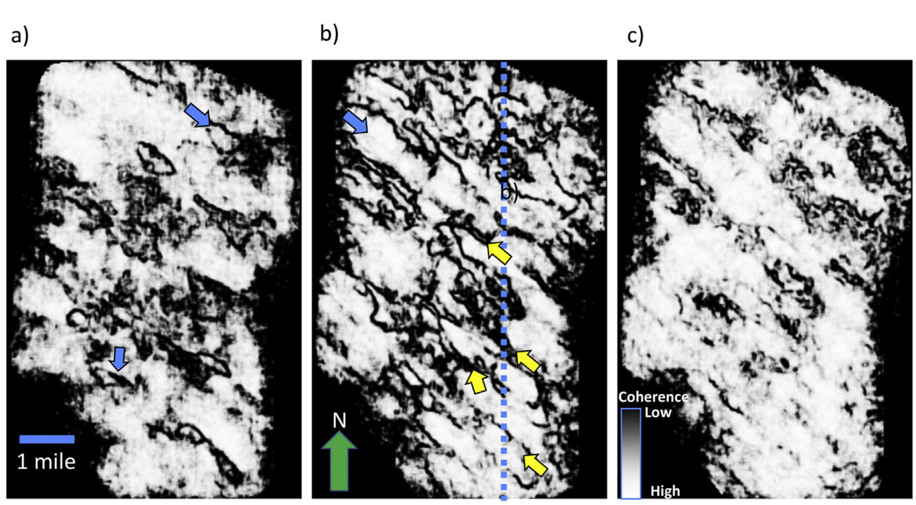

Fig. 6. Stratal slices of the coherence attribute with respect to the Nugget Sandstone reflector. The eolian dune lineaments, starts appearing 66 ms below Nugget (a), become conspicuous features around 42 ms (b) and start vanishing about 26 ms below Nugget (c). Note the blue arrow indicates the interdunal whereas the yellow arrow indicates the well developed sand dunes. (For interpretation of the references to color in this figure legend, the reader is referred to the Web version of this article.)

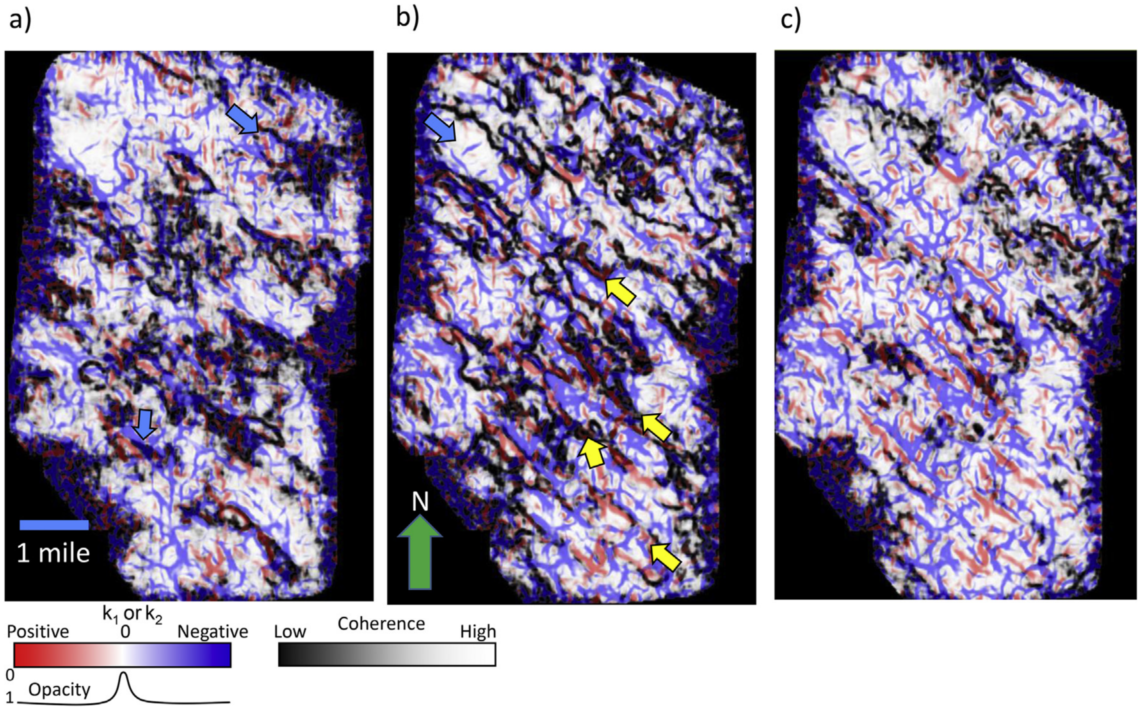

Fig. 7. Stratal slices of the curvature attribute with respect to the Nugget Sandstone reflector. The peculiar geologic features begin to appear 66 ms below Nugget (a), become prominent around 42 ms (b) and then start disappearing about 26 ms below Nugget (c). Note the blue arrow indicates the interdunal whereas the yellow arrow indicates the well developed sand dunes. (For interpretation of the references to color in this figure legend, the reader is referred to the Web version of this article.)

with P-impedance in SOM as input attributes. Roy et al. (2013) used above mentioned GLCM attributes and discriminated between producing and non-producing carbonate facies with SOM classification method. In this paper we have used distance preserving SOM method, which was first used by Zhao et al. (2016). Fig. 9 shows SOM classified 120 seismic facies co-rendered with coherence displayed at deep, middle and shallow stratal slices. Here, the proximal colors on the color bar indicate similar facies, which can be related to similar rock types. The hot colored (yellow and red) facies correspond to the low P-impedance values or dunal sandstone, whereas the cold (blue) colored facies correspond to high impedance values or interdunal deposits. The change in the gradation of colors might indicate the mixing of the two facies.

4. Discussions

The deep stratal slice (66 ms below Nugget Sandstone, Fig. 9a) indicates that in the central part of the survey, sand dunes are building up; dunal sandstones are indicated by hot colors, and the dark coherence demarcates the spatial extent of dunal deposits. There are few blue colored anomalies (indicated by white arrows) which are enclosed by low coherence anomalies. We hypothesize that these are the interdunal areas which were lowest in elevation, when sand dunes were building up on the two sides. Several episodes of rain could have caused the ephemeral lakes to form, and once lakes dried up, they left off evaporites behind. The petrophysical analysis of AGI-2-18 and Keller 1–12 wells indicates that the Nugget Sandstone formation is vertically heterogeneous. Although the top and base of the Nugget Sandstone formation could be laterally correlated across the wells based on the overall signatures of common well logs (suggestive of less external heterogeneity), there is a significant amount of internal heterogeneity present. Based on the multi-mineralogical solution, the AGI 2–18 well shows the significant proportion of quartz and less clay compared to the Keller 1–12 well. In addition, AGI 2–18 well shows the presence of a 50 ft thick layer of evaporite (halite and anhydrite) in the middle of Nugget Sandstone formation, which is not present in the Keller 1–12 well. This could be due to lateral variations of facies. Presence of evaporites, such as halite and anhydrite at the same depth can be explained in terms of their deposition through secondary fluid flow processes. A comparison of multi-mineralogical solution between AGI 2–18 and Keller 1–12 wells suggests that the former well is more representative of sand dunal environment, whereas the other one may represent more of an interdunal environment. Velocity of halite is much higher than sandstone, whereas the density of halite is lower than sandstone; which leads to slightly higher (but comparable) range of impedance in halite compared to sandstone. In the above mentioned 50 ft evaporite layer in AGI 2–18, anhydrite exists along with halite, where the high velocity and high density of anhydrite leads to a higher impedance of this layer compared to the adjacent sandstone layer. The middle stratal slice of seismic facies volume (Fig. 9b) indicates that the dunal sandstones are well developed. Fig. 8c, displays GLCM homogeneity attribute on the middle stratal slice with bump map. We can compare Fig. 8c with the modern day analog Fig. 2c. The lineations observed with attribute only indicate that the wind direction can be from NE or SW direction, with this figure we extend our interpretation. In Fig. 8c, we marked a red arrow where one sand dune is joining the adjacent sand dune. The northeast directional curving of sand dune, indicated it to the windward direction.

Curvature, coherence, homogeneity show clear trend of NW-SE trending lineaments, which we correlated to sand dunes. Here, we attempt to find the direction of these lineaments, and quantify the wind direction. We use the most positive curvature (k_1) volume in the zone of interest (120 ms window, see green dotted lines in Fig. 5a) and we apply Ant Tracking workflow to track the connected discontinuity surfaces (Silva et al., 2005). These discontinuity surfaces mostly correspond to the changes in k_1 from positive to negative. A lineation corresponding to the sand dunes appears as a discontinuity surface (Fig. 10a). Further, we compute the strike of these discontinuity surfaces. In order to focus on the lineation of NW-SE direction, we filtered the small discontinuities N to E direction. We compute the wind

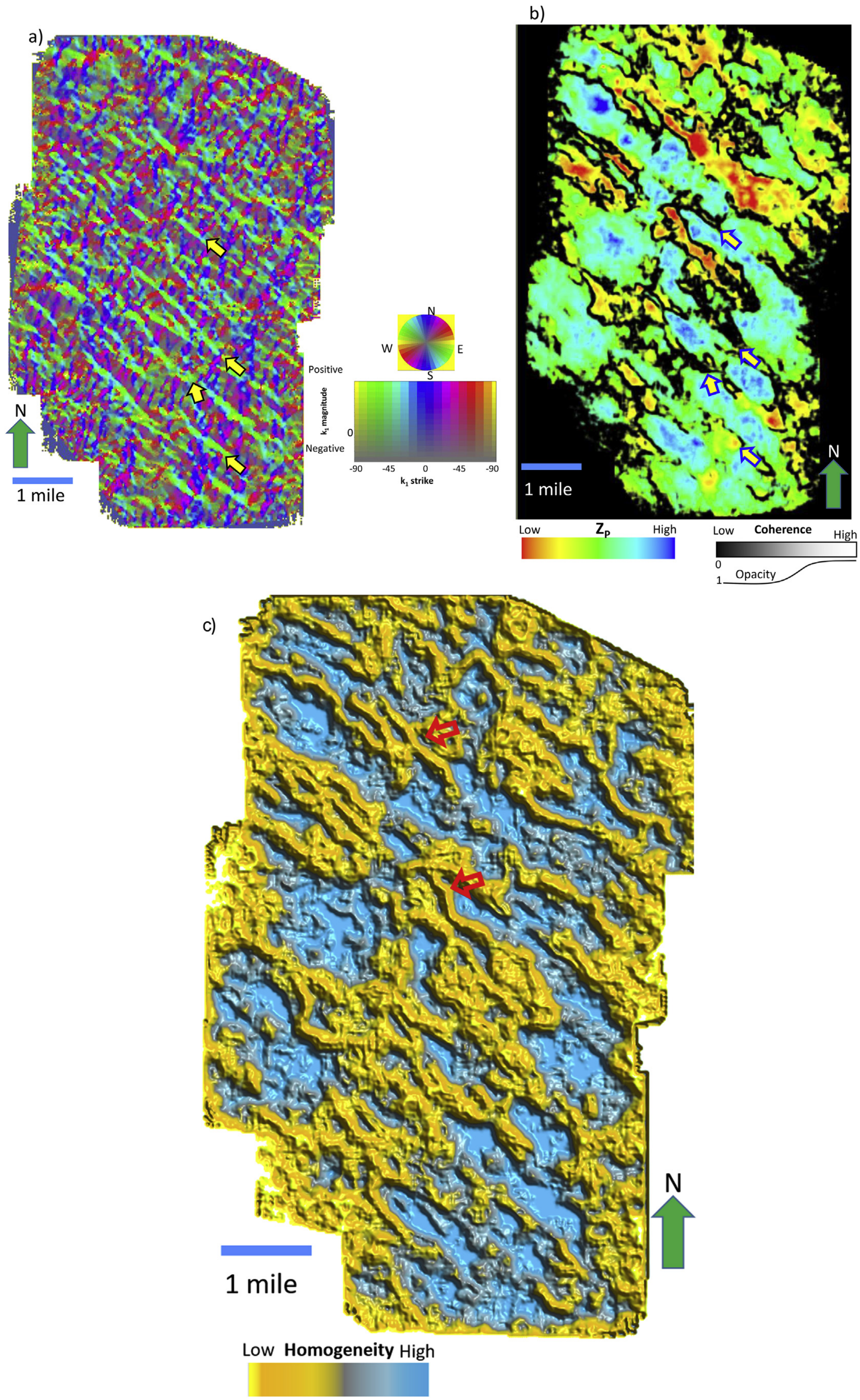

Fig. 8. Different attributes displayed at the middle stratal slice (64 ms below Nugget). (a). Strike of most positive principal curvature k_1 is blended with magnitude of k_1, notice most of the lineation are trending in NW-SE direction. (b) P-impedance co-rendered with coherence, notice that the low P-impedance values are bounded by low coherence anomaly. (c) GLCM homogeneity with bump map. Note the yellow arrow (same location as Fig. 5 and 6) indicates the well developed sand dunes. (For interpretation of the references to color in this figure legend, the reader is referred to the Web version of this article.)

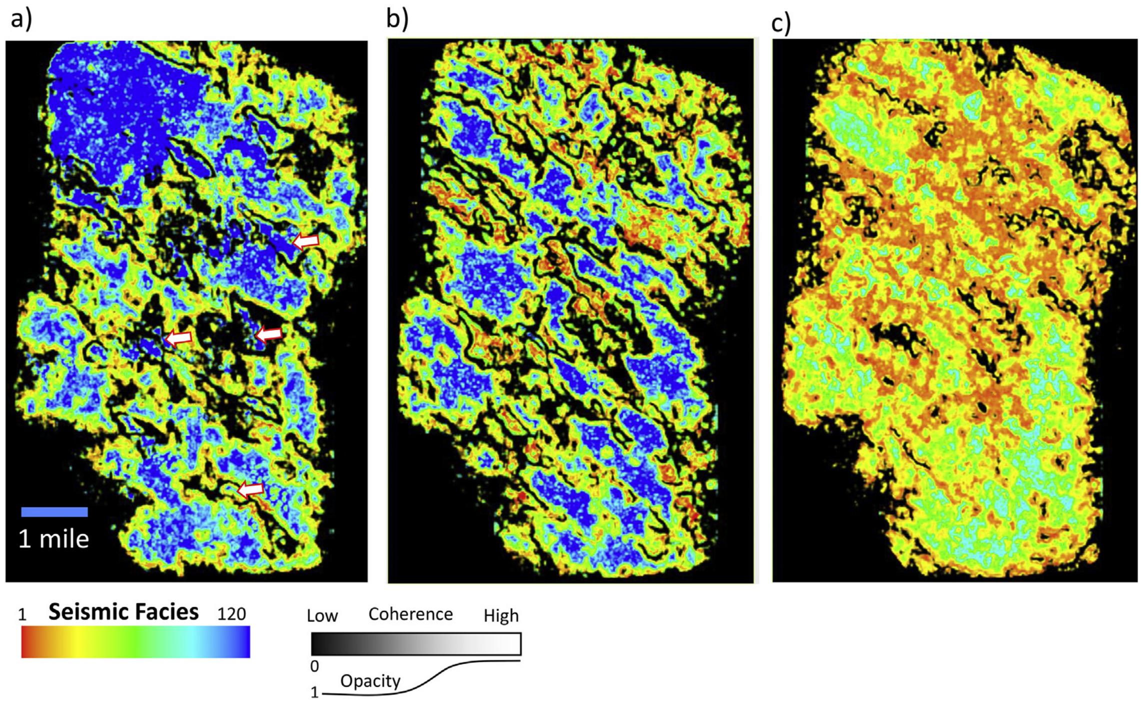

Fig. 9. Stratal slices of the seismic facies, generated with the self organizing map (SOM) algorithm, with respect to the Nugget Sandstone reflector. The eolian dunes lineaments begin to appear 66 ms below Nugget (a), become prominent around 42 ms (b) and then start disappearing about 26 ms below Nugget (c). Based on the correlation of P-impedance and seismic facies, we observed that, the blue colored facies are interdunal deposits whereas the red colored facies are dunal deposit. (For interpretation of the references to color in this figure legend, the reader is referred to the Web version of this article.)

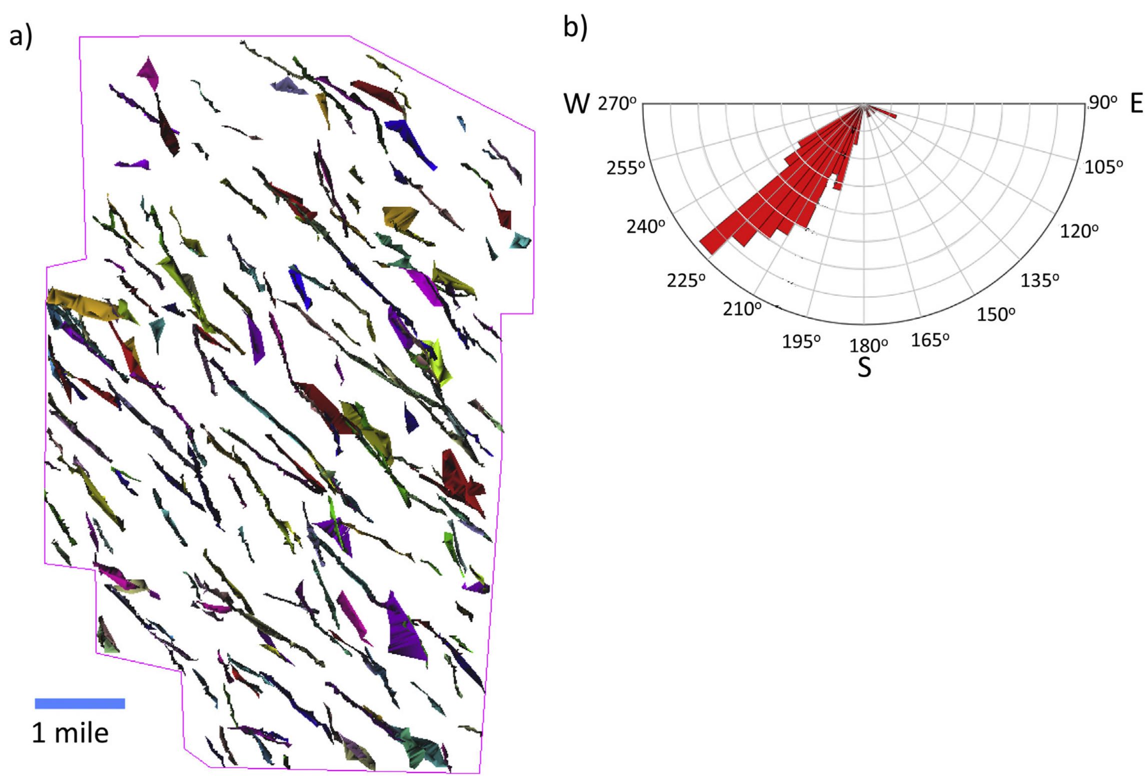

Fig. 10. (a)The discontinuity surfaces obtained by applying Ant Track workflow (Silva et al., 2005) on curvature k_1 volume (Fig. 6). Note that all the small north to east striking lineaments were filtered out. (b) The rose diagram, showing the derived direction; which is simply the perpendicular direction to the strike of the lineaments in Fig. 9a.

direction by adding 90° to the strike direction of these lineation. The computed wind direction (blowing towards), a range of values from N195° to N240° (Fig. 10b). The highest concentration of points is around N225°.

5. Conclusions

The Nugget Sandstone is an eolian deposit, characterized by dunal and interdunal deposits. High correlation of well to seismic tie, confirms that the lineaments seen in the seismic data are within the Nugget Sandstone. The petrophysical analysis indicated that the Nugget Sandstone interval consists of sandstone (dunal deposits) and clay along with carbonates (interdunal deposits). Multi-well analysis suggests that the overall lithology of the Nugget sandstone formation may be uniform (i.e. sandstone); however, there is a significant amount of internal heterogeneity present in the wells that can be correlated laterally. Coherence and curvature (seismic) attributes show NW-SE lineaments in Nugget Sandstone, we hypothesize that these lineaments correspond to the transverse dunes, and the predominant paleo-wind direction would be NE-SW. Acoustic impedance and petrophysical analysis helped in discriminating dunal and interdunal deposits. Nugget Sandstone formation appears to have a good potential as a carbon storage reservoir based on its lithology, porosity, fluid saturation, and vertical and lateral extent.

(b) Illustration showing 2D curvature of a curved line. Anticlinal features show positive curvature anomaly, whereas synclinal features show a negative curvature anomaly and planar features (horizontal or dipping) show no curvature anomaly. (c). The illustration shows structural curvature anomaly at an antiform and a synform. The most positive (k_1) and most negative principal curvatures (k_2) anomalies will track the hinge lines which are areas of maximum strain (after Mai et al., 2009).

Acknowledgements

This seismic data was obtained with the research grant provided by the United States Department of Energy: Contract No: DE-FE0023328. We thank CGG GeoSoftware for Hampson-Russell, Schlumberger for Petrel, and IHS for Petra software licenses provided to the University of Texas of the Permian Basin for research and education. We also thank Attribute Assisted Seismic Processing & Interpretation Consortium for providing AASPI software, which was used to compute seismic attributes. We would like to thank Ms. Fatimah Adelekan, Ms. Yvonne Iwo-Brown and Ms. Joanna Walker for their help with this project.

References

Archie, G.E., 1942. The electrical resistivity log as an aid in determining some reservoir characteristics. Pet. Trans. AIME 146, 54–62. https://doi.org/10.2118/942054-G.

ASTER, 2005. NASA's satellite image of Rub' al Khali, Arabia. 2017. https://www.nasa.gov/multimedia/imagegallery/image_feature_1200.html accessed 10 December 10.

Campbell-Stone, E., Lynds, R., Frost, C., Becker, T.P., Diem, B., 2011. The Wyoming carbon underground storage project: geologic characterization of the Moxa arch and rock Springs uplift. Energy Procedia 4, 4656–4663.

Chan, M.A., Archer, A.W., 2000. Cyclic eolian stratification on the Jurassic Navajo sandstone, zion National Park: Periodicities and implications for paleoclimate. In: In: Sprinkel, D.A., Chidsey Jr.T.C., Anderson, P.B. (Eds.), Geology of Utah's Parks and Monuments, vol. 28. Utah Geological Association Publication, pp. 607–617.

Chopra, S., Marfurt, K.J., 2010. Integration of coherence and volumetric curvatures images. Lead. Edge 29, 1092–1107.

Chopra, S., Marfurt, K., 2007. Seismic Attributes for Prospect Identification and Reservoir Characterization. SEG Geophysical Developments No. 11https://doi.org/10.1190/1.9781560801900.

Grana, D., Verma, S., Pafeng, J., Lang, X., Sharma, H., Wu, W., Campbell-Stone, E., Ng, K., Alvarado, V., Mallick, S., Kaszuba, J., 2017. A rock physics and seismic reservoir characterization study of the Rock Springs Uplift, a carbon dioxide sequestration site in Southwestern Wyoming. Int. J. Greenh. Gas Contr. 63, 296–309. https://doi.org/10.1016/j.ijggc.2017.06.004.

Khoudaiberdiev, R., Bennett, C., Bhatnagar, P., Verma, S., 2017. Seismic Interpretation of Cree Sand Channels on the Scotian Shelf: 87th SEG Annual Meeting. SEG Technical Program Expanded Abstracts 2008-2012. https://doi.org/10.1190/segam2017-17742372.1.

Kulyapin, P., Sokolova, T.F., 2014. A case study about integrated Petrofacies characterization and interpretation of depositional environment of the bakken shale in the Williston basin, north America formation evaluation and rock physics modeling of the bazhenov shale. Petrophysics 55 (3), 211–218.

Lindquist, S.J., 1983. Nugget Sandstone formation reservoir characteristics affecting production in the overthrust belt of Southwestern Wyoming. Soc. Petrol. Eng. 35, 1355–1365. https://doi.org/10.2118/10993-PA. SPE-10993-PA.

Loope, D.B., Rowe, C.M., 2003. Long-lived pluvial episodes during deposition of the Navajo Sandstone. J. Geol. 111, 223–232.

Mai, H.T., Marfurt, Chávand ez-Pérez, S., 2009. Coherence and volumetric curvatures and their spatial relationship to faults and folds, an example from Chicontepec Basin, Mexico: 79th SEG Annual Meeting. SEG Tech. Progr. Expand. Abstr. 1063–1067. https://doi.org/10.1190/1.3255033.

Mallick, S., Adhikari, S., 2015. Amplitude-variation-with-offset and prestack-waveform inversion: a direct comparison using a real data example from the Rock Springs Uplift. Wyoming, USA: Geophysics 80 (2), B45–B59.

Matos, M.C., Léo Osorio, P., Johann, P.R., 2007. Unsupervised seismic facies analysis using wavelet transform and self-organizing maps. Geophysics 72 (1), P9–P21. https://doi.org/10.1190/1.2392789.

Mitchell, W.K., Nelson, R.J., 1988. A Practical approach to statistical log analysis. In: Paper S, Transactions: SPWLA 29th Annual Logging Symposium, SPWLA-1988-S.

Moss, B., Harrison, R., 1985. Statistically valid log analysis method improves reservoir description. In: SPE Offshore Europe Annual Meeting, SPE-13981, . https://doi.org/10.2118/13981-MS.

National Park Services, 2016. Appalachian Paleogeography. https://www.nature.nps.gov/geology/education/education_graphics.cfm, Accessed date: 10 December 2017.

Parrish, J.T., Peterson, F., 1988. Wind directions predicted from global circulation models and wind directions determined from eolian sandstones of the western United States - a comparison. Sediment. Geol. 56, 261–282.

Qi, J., Li, F., Marfurt, K., 2017. Multiazimuth coherence. Geophysics 82 (6), O83–O89. https://doi.org/10.1190/geo2017-0196.1.

Qi, J., Zhang, B., Zhou, H., Marfurt, K.J., 2014. Attribute expression of fault-controlled karst—fort Worth basin, Texas. A tutorial: Interpretation 2 (3), SF91–SF110.

Rider, M., Kennedy, M., 2011. The Geological Interpretation of Well Logs, third ed. Rider-French Consulting Limited, pp. 432.

Roy, A., Dowdell, B.L., Marfurt, K.J., 2013. Characterizing a Mississippian tripolitic chert reservoir using 3D unsupervised and supervised multiattribute seismic facies analysis: an example from Osage County, Oklahoma. Interpretation 1 (2) SB109-SB124. https://doi.org/10.1190/INT-2013-0023.1.

Saraswat, P., Sen, M.K., 2012. Artificial immune-based self-organizing maps for seismic-facies analysis. Geophysics 77 (4), O45–O53.

Savre, W.C., 1963. Determination of a more accurate porosity andMineral composition in complex lithologies with the use of the sonic, neutron, and density surveys. J. Petrol. Technol. 15 (6), 945–959 Paper SPE-617.

Sharma, H., Mallick, S., Verma, S., Campbell, Erin, 2018. Azimuthal anisotropy analysis of multiazimuth P-wave seismic data — an example from the Rock Springs Uplift, Wyoming, USA. Interpretation 6 (3), T649–T666. https://doi.org/10.1190/INT-2017-0230.1.

Silva, Celina C., Marcolino, C.S., Lima, F.D., 2005. Automatic fault extraction using ant tracking algorithm in the Marlim South Field, Campos Basin. In: 75th Annual International Meeting. SEG, pp. 857–860 Expanded Abstracts.

Surdam, R.C., 2013. Geological CO2 Storage Characterization: the Key to Deploying Clean Fossil Energy Technology. Springer.

Thyne, G.D., Tomasso, M., Bywater-Reyes, S.V., Budd, D.A., Reyes, B.M., 2010. Characterization of porosity and permeability for CO_2 sequestration models in the Mississippian Madison Group, Moxa Arch-LaBarge Platform, southwestern Wyoming. Rocky Mt. Geol. 45 (2), 133–150.

Verma, S., Campbell-Stone, E., Sharma, H., Mallick, S., Grana, D., 2016. Seismic attribute illumination of the Moxa Arch: a probable site for carbon sequestration. In: 86th Annual International Meeting. SEG, Expanded Abstracts, pp. 1874–1878.

Zhao, T., Zhang, J., Li, F., Marfurt, K.J., 2016. Characterizing a turbidite system in Canterbury Basin, New Zealand, using seismic attributes and distance-preserving self-organizing maps. Interpretation 4 (1), SB79–SB89. https://doi.org/10.1190/INT-2015-0094.1.